

Pattern Formation in Double-Layer Kerr Resonators with Coupled Modes

Antoine Bois and Joyce K. S. Poon

*The Edward S. Rogers Sr. Department of Electrical & Computer Engineering,
University of Toronto, Toronto, ON M5S 3G4, Canada*

**Corresponding author: antoine.bois@mail.utoronto.ca*

A double-layer Kerr resonator in which both coupled modes are excited and interact with each other via incoherent cross-phase modulation is investigated to reveal stable localized solutions beyond the usual formation mechanism involving a single mode. Periodic solutions from modulational instability are found to occur at a slight penalty on the nonlinear efficiency, but they stabilize the spatial dynamics, leading to dissipative solitons in previously unattainable regimes. Numerical simulations show paired breather solitons in addition to temporally stable solutions. The results demonstrate coupled modes can increase the stability of Kerr frequency comb generation.

The study of localized light patterns in passive Kerr resonators has recently experienced a renewal of interest for its relevance to coherent frequency comb generation. In such resonators, dissipative Kerr solitons are able to arise spontaneously from a single monochromatic continuous-wave (cw) input. Their dynamics are well documented [1–7]. In short, in cavities with anomalous dispersion, dissipative solitons have been understood to emerge from the homoclinic orbit of a stable homogeneous steady state (HSS) passing asymptotically close, in phase space, to a stable periodic pattern, itself originating from modulational instability (MI). Compared to periodic patterns by themselves, solitons vastly broaden the spectrum of the optical field, making them preferred for frequency combs.

In a standard resonator, this soliton formation mechanism takes place with the lower intracavity power HSS in the bistable region of a nonlinear resonance. This metastability of the HSS causes stability issues in the practical implementations of Kerr combs [8, 9]. In the upper branch of the bistability, periodic patterns tend to progress into spatiotemporal chaos (sometimes also called optical turbulences) [10], while in the low intracavity power monostable regime, spatial eigenvalues of the HSS are generally found unsuitable for this homoclinic orbit to occur, despite a HSS briefly co-existing with a subcritical periodic solution [5].

In this Letter, we investigate the formation dynamics of both temporal dissipative solitons and periodic patterns in a resonator formed by two coupled guiding layers that support two waveguide modes of similar polarization. We show that incoherent cross-phase modulation (XPM) between the two modes leaves the onset of MI mostly intact and is able to modify the spatial eigenvalues to extend the range of input parameters that support heteroclinic coupling of a HSS to a periodic pattern. Our analysis accounts for both coupled modes simultaneously, in contrast to recent works that only study and use one of the coupled modes for dispersion engineering [11, 12].

In our case, a coupled structure is employed mainly to circumvent the issue of modal anticrossings typical to multimode resonators. This phenomenon arises when two modes are simultaneously close to resonance, due to

coupling between them that perturbs both their phases and amplitudes and thus prevents a resonance degeneracy, as described by standard coupled-mode theory [13]. Here, we use the eigensolutions of the coupled propagation equations as a basis. In a double-layer resonator, this conveniently corresponds to the symmetric and anti-symmetric modes of the coupled structure. In addition to the disappearance of anticrossings, this basis offers an increased XPM efficiency compared to higher order modes, a relative ease of coupling from a bus waveguide, and a broad range of possible dispersion engineering enabled by the mode coupling term, κ , designed through the separation between and dimensions of the guiding layers [11, 12]. Fig. 1 shows the proposed device in the form of a microring, including the input/output bus waveguide. Such a device can be implemented in multi-layer silicon nitride or silicon nitride-on-silicon integrated photonic platforms [14, 15].

Achieving co-resonance is straightforward. Neglecting the second-order dispersion, for a fixed detuning of the symmetric mode u , the difference in detunings $\Delta\theta = \theta_u - \theta_v$ (with anti-symmetric mode v) for successive resonances n is

$$\Delta\theta_{n+1} = (\Delta\theta_n + 2\pi(n_g^v - n_g^u)/n_g^u) \bmod 2\pi, \quad (1)$$

where n_g is the group index. For instance, for transverse electric (TE) polarized light and nominally single-mode Si_3N_4 waveguides with heights around 600 nm and inter-layer separations about 400 nm, $n_g^v - n_g^u$ is on the order of 10^{-1} for wavelengths near 1310 nm, and $n_g^u \simeq 2$ for a 0.016π phase step between resonances. A similar analysis can be performed for the anti-symmetric mode by interchanging u with v in the denominator.

Turning our attention to the dynamics of the system under study, we introduce the standard mean-field Lugiato-Lefever equation (LLE) [1] to describe the nonlinear propagation of the slowly varying field envelopes. Using the normalization of [16], modified to include the XPM interaction and mismatch in group velocities, the LLE becomes

$$\partial_t u = -(1 + i\theta_u)u + i(|u|^2 + 2|v|^2)u + S_u - i\eta_u \partial_\tau^2 u - \delta \partial_\tau u, \quad (2a)$$

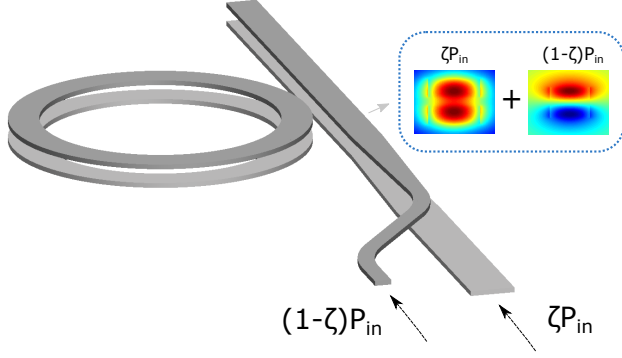


FIG. 1: A microring resonator consisting of two guiding layers supports symmetric and anti-symmetric modes for TE and transverse magnetic (TM) polarizations. Light launched into the wider (narrower) waveguide converts adiabatically to the symmetric (anti-symmetric) mode of the vertical bus coupler for selective modal excitation. The waveguides then couple evanescently to the resonator with low cross-talk due to the phase matching imposed by the directional coupler. The splitting ratio, ζ , can be implemented either on- or off-chip. The optical input is monochromatic and has power P_{in} .

$$\partial_t v = -(1+i\theta_v)v + i(|v|^2 + 2|u|^2)v + S_v - i\eta_v \partial_\tau^2 v + \delta \partial_\tau v, \quad (2b)$$

with t as the slow time (on the scale of the optical round-trip time), τ as the fast time (in a reference frame traveling at the average of the group velocities), $\theta_{u,v}$ as the detuning with the closest linear resonance, $S_{u,v}$ as the amplitude of the coherent cw pump, and $\eta_{u,v}$ and δ , the second-order dispersion and extraneous first-order dispersion respectively, being defined as a ratio to the average of the absolute values for the two modes. The first term on the right side relates to the normalized losses including propagation and coupling, here assumed similar for both modes. We choose to work in a strongly coupled regime such that the coherent four-wave mixing term $\exp(\pm i4\kappa t)$ oscillates rapidly with t to average to zero and can be neglected. The mechanism presented here therefore depends only on *incoherent* XPM.

The homogeneous solutions of Eq. 2 are instructive as a starting point for the formation of patterned solutions. This is done by setting all derivatives to zero and leads

$$\begin{vmatrix} -\lambda_t - (1+i\theta_u) + i(\eta_u \Omega^2 - \delta \Omega) + 2i(|u|^2 + |v|^2) & i|u|^2 & 2i|u||v| & 2i|u||v| \\ -i|u|^2 & -\lambda_t - (1-i\theta_u) - i(\eta_u \Omega^2 - \delta \Omega) - 2i(|u|^2 + |v|^2) & -2i|u||v| & -2i|u||v| \\ 2i|u||v| & 2i|u||v| & -\lambda_t - (1+i\theta_v) + i(\eta_v \Omega^2 + \delta \Omega) + 2i(|u|^2 + |v|^2) & i|v|^2 \\ -2i|u||v| & -2i|u||v| & -i|v|^2 & -\lambda_t - (1-i\theta_v) - i(\eta_v \Omega^2 + \delta \Omega) - 2i(|u|^2 + |v|^2) \end{vmatrix} = 0, \quad (4)$$

to

$$X_u = Y_u^3 - 2(\theta_u - 2Y_v)Y_u^2 + [(\theta_u - 2Y_v)^2 + 1]Y_u, \quad (3a)$$

$$X_v = Y_v^3 - 2(\theta_v - 2Y_u)Y_v^2 + [(\theta_v - 2Y_u)^2 + 1]Y_v, \quad (3b)$$

where $X_{u,v} \equiv |S_{u,v}|^2$, the intensity of each cw input, and $Y_u \equiv |u|^2$, $Y_v \equiv |v|^2$. At first glance, the effect of XPM is to act as an additional effective detuning to $\theta_{u,v}$. However, the dynamical nature of Y_u and Y_v means that they are not independent of each other, and therefore neither is this control over the detuning. Approaching the resonance from the stable high frequency side ($\theta_{u,v} < 0$), despite X_u and X_v being potentially similar in magnitude, the mode with more power ends up overwhelmingly dominating the resonance. This is illustrated in Fig. 2, where both are plotted on the same scale. This turns out

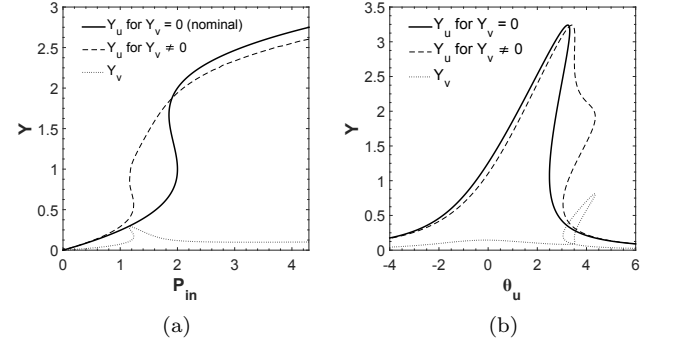


FIG. 2: Intracavity power of the homogeneous solutions as a function of (a) input pump power $P_{in} = X_u + X_v$, for $X_u/X_v = 3$ and fixed detunings $\theta_u = 2$, $\theta_v = \theta_u + 0.2$; and (b) input detuning θ_u , for $\theta_v = \theta_u + 0.2$ and $X_u = 3.24$, $X_u/X_v = 3$.

to be a necessary condition for the stability of the HSS, at least to homogeneous perturbations. If both modes were to be sustained at close to full resonance, then any slight perturbation in any direction would strongly affect the XPM, in turn modifying the resonance condition and intracavity power of the second mode, and thus further destabilizing the original mode and amplifying that initial perturbation. This is formalized mathematically by writing small perturbations $\varepsilon \propto \exp(\lambda_t t + i\Omega \tau)$ into Eqs. 2a and 2b. Keeping only the linear terms and solving for the non-trivial solutions of $[\varepsilon_u, \varepsilon_u^*, \varepsilon_v, \varepsilon_v^*]^T$ leads to

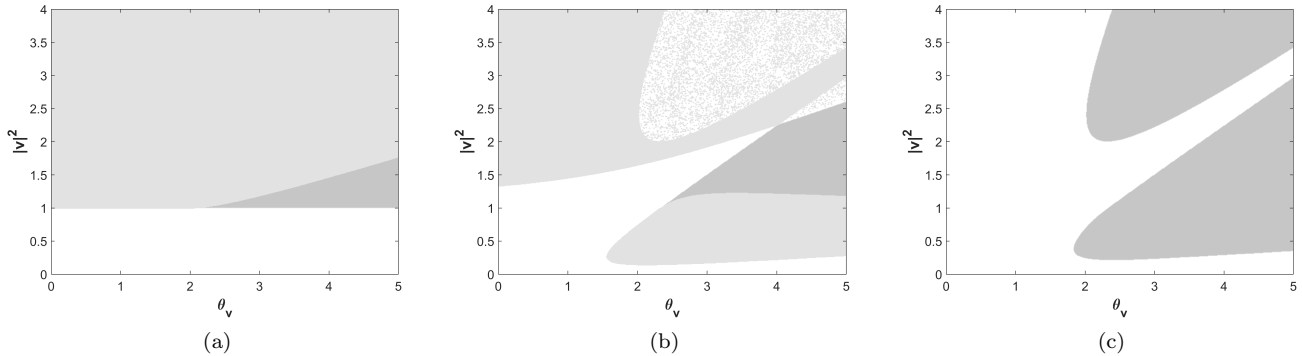


FIG. 4: Regions of the parameter space $(\theta_v, |v|^2)$ with qualitatively different eigenspectra for (a) $|u|^2 = 0$, $\delta = 0$; (b) $|u|^2 = 0.6$, $\delta = 0$; and (c) $|u|^2 = 0.6$, $\delta = 4 \times 10^{-22}$. Other parameters are fixed as $\eta_u = 5$, $\eta_v = -1$, $\theta_u = 3$. The white region corresponds to all the eigenvalues being complex, the light gray region to a subset being purely imaginary, and the dark gray region to a subset being purely real. The upper right quadrant of (b) shows fast transitions between the white and light gray regions.

ics, which are expected to be complex due to multiple bistabilities that can be triggered by large amplitude extents of the localized patterns.

Nonetheless, by direct simulation of Eq. 2 with a split-step Fourier method [18], we find that soliton formation occurs for a large set of parameters that are robust to second-order dispersion or group velocity mismatch. Fig. 5 shows examples of such solutions in normalized units. Physically, Fig. 5 (a) and (b) correspond to a microring with two Si_3N_4 layers, a radius of $150 \mu\text{m}$, a vertical separation of 400 nm , waveguide widths of 850 nm , waveguide heights of 600 nm , and a quality factor of 9.06×10^5 . At a wavelength of 1310 nm , the TE polarized symmetric and anti-symmetric modes are computed to have group indices of 1.97 and 2.05 , respectively, and second-order dispersions of $-510 \text{ ps nm}^{-1} \text{ km}^{-1}$ and $44 \text{ ps nm}^{-1} \text{ km}^{-1}$, respectively. The external cw inputs are 50 mW and 100 mW , and the nonlinear coefficient, γ , is $1.645 \text{ W}^{-1} \text{ m}^{-1}$.

In Fig. 5 (c) and (d), the microring radius is decreased to $100 \mu\text{m}$, and the input power of the symmetric mode increased to 80 mW . In terms of the sensitivity of soliton pairing to group velocity mismatch, through a perturbation of the solutions, we observe a return to a paired state analogous to soliton trapping in birefringent optical fibers [19], indicating the soliton pairing is stable.

In conclusion, we have shown the formation dynamics of periodic patterns and solitons in a double-layer Kerr resonator with two coupled modes interacting via XPM are modified compared to those from a single mode. The new degrees of freedom are promising for the practical generation of Kerr frequency combs from cavity solitons, achieved through a stabilization of spatial dynamics. Future investigations can include the effects caused by higher order dispersion and the analytical studies of MI and other bifurcations in coupled structures.

-
- [1] L. A. Lugiato and R. Lefever, *Phys. Rev. Lett.* **58**, 2209 (1987).
- [2] A. Scroggie, W. Firth, G. McDonald, M. Tlidi, R. Lefever, and L. A. Lugiato, *Chaos, Solitons & Fractals* **4**, 1323 (1994).
- [3] Y. K. Chembo and N. Yu, *Phys. Rev. A* **82**, 033801 (2010).
- [4] C. Godey, I. V. Balakireva, A. Coillet, and Y. K. Chembo, *Phys. Rev. A* **89**, 063814 (2014).
- [5] P. Parra-Rivas, D. Gomila, M. A. Matías, S. Coen, and L. Gelens, *Phys. Rev. A* **89**, 043813 (2014).
- [6] P. Parra-Rivas, D. Gomila, E. Knobloch, S. Coen, and L. Gelens, *Opt. Lett.* **41**, 2402 (2016).
- [7] T. Hansson and S. Wabnitz, *Nanophotonics* (2016).
- [8] X. Yi, Q.-F. Yang, K. Youl, and K. Vahala, *Opt. Lett.* **41**, 2037 (2016).
- [9] M. Karpov, H. Guo, E. Lucas, A. Kordts, M. Pfeiffer, G. Lichachev, V. Lobanov, M. Gorodetsky, and T. Kippenberg, arXiv preprint arXiv:1601.05036 (2016).
- [10] K. Ikeda, H. Daido, and O. Akimoto, *Phys. Rev. Lett.* **45**, 709 (1980).
- [11] M. Soltani, A. Matsko, and L. Maleki, *Laser Photon. Rev.* **10**, 158 (2016).
- [12] S. Kim, K. Han, C. Wang, J. A. Jaramillo-Villegas, X. Xue, C. Bao, Y. Xuan, D. E. Leaird, A. M. Weiner, and M. Qi, arXiv preprint arXiv:1607.01850 (2016).
- [13] Y. Liu, Y. Xuan, X. Xue, P.-H. Wang, S. Chen, A. J. Metcalf, J. Wang, D. E. Leaird, M. Qi, and A. M. Weiner, *Optica* **1**, 137 (2014).
- [14] W. D. Sacher, Z. Yong, J. C. Mikkelsen, A. Bois, Y. Yang, J. C. Mak, P. Dumais, D. Goodwill, C. Ma, J. Jeong, E. Bernier, and J. K. Poon, in *CLEO: Science and Innovations* (Optical Society of America, 2016) pp. JTh4C-3.
- [15] W. D. Sacher, Y. Huang, G.-Q. Lo, and J. K. Poon, J.

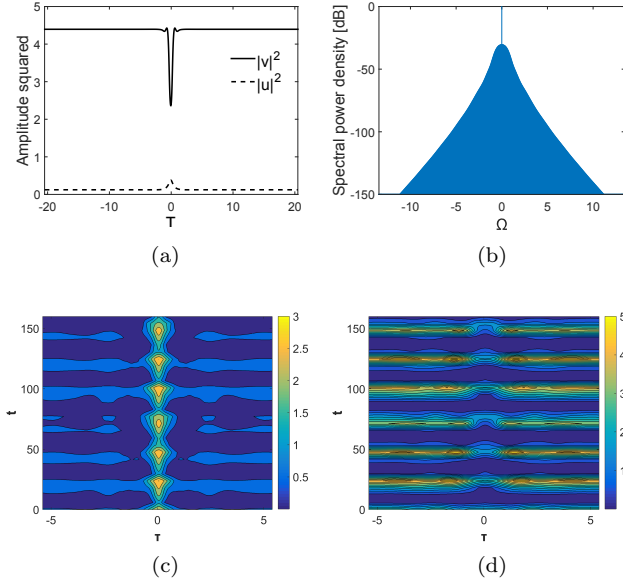


FIG. 5: (a) Temporally stable dark/bright soliton pair showing $|u|^2$ and $|v|^2$, and (b) amplitude spectrum of the high intracavity power component v , for $\eta_u = 1.84$, $\eta_v = -0.16$, $\theta_u = \theta_v = 4$, $S_u = 1.76$, $S_v = 2.49$, and $\delta = 4.37 \times 10^{-22}$; (c)–(d) temporal dynamics of a breather dark/bright soliton pair, showing $|u|^2$ and $|v|^2$ respectively, for $\eta_u = 1.84$, $\eta_v = -0.16$, $\theta_u = \theta_v = 3$, $S_u = 1.82$, $S_v = 2.03$, and $\delta = 4.37 \times 10^{-22}$.

Lightwave Technol. **33**, 901 (2015).

- [16] F. Leo, S. Coen, P. Kockaert, S.-P. Gorza, P. Emplit, and M. Haelterman, title (ISO 4) Nat. Photon. **4**, 471 (2010).
- [17] P. Colet, M. A. Matías, L. Gelens, and D. Gomila, Phys. Rev. E **89**, 012914 (2014).
- [18] G. P. Agrawal, *Nonlinear fiber optics* (Academic press, 2007).
- [19] M. Islam, C. Poole, and J. Gordon, Opt. Lett. **14**, 1011 (1989).